Science of the Total Environment 680 (2019) 23–34

Contents lists available at ScienceDirect

Science of the Total Environment

journal homepage: www.elsevier.com/locate/scitotenv

Modes of action and adverse effects of gamma radiation in an aquatic macrophyte *Lemna minor*

Li Xie [a,b,c,*], Knut Asbjørn Solhaug [b,c], You Song [a,c], Dag Anders Brede [b,c], Ole Christian Lind [b,c], Brit Salbu [b,c], Knut Erik Tollefsen [a,b,c,*]

[a] Norwegian Institute for Water Research (NIVA), Section of Ecotoxicology and Risk Assessment, Gaustadalléen 21, N-0349 Oslo, Norway
[b] Norwegian University of Life Sciences (NMBU), Faculty of Environmental Sciences and Natural Resource Management (MINA), P.O. Box 5003, N-1432 Ås, Norway
[c] Centre for Environmental Radioactivity, Norwegian University of Life Sciences (NMBU), Post box 5003, N-1432 Ås, Norway

HIGHLIGHTS

- Mode of action and adverse effects of gamma radiation was demonstrated in the aquatic plant *Lemna minor*.
- Gamma radiation displays both dose rate-dependent and target-specific responses on *L. minor*
- DNA damage and ROS formation as the main mode of actions
- Causal linkage between MoA and adverse outcomes were developed into a network of toxicity pathways.

GRAPHICAL ABSTRACT

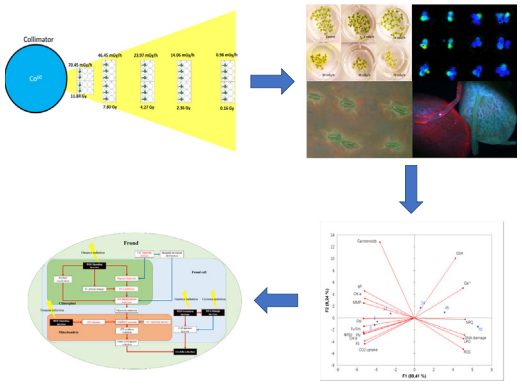

ARTICLE INFO

Article history:
Received 4 March 2019
Received in revised form 1 May 2019
Accepted 2 May 2019
Available online 7 May 2019

Editor: Daniel Wunderlin

Keywords:
Gamma radiation
Aquatic plant
Mode of action
Adverse effect

ABSTRACT

High dose rates of ionizing radiation have been reported to cause adverse effects such as reduction in reproduction and growth, and damage to protein and lipids in primary producers. However, the relevant effects of ionizing radiation are still poorly understood in aquatic plants. This study was intended to characterize the biological effects and modes of action (MoAs) of ionizing radiation using gamma radiation as the prototypical stressor and duckweed *Lemna minor* as a model organism. *Lemna minor* was exposed to 1, 14, 24, 46, 70 mGy/h gamma radiation dose rates from a cobalt-60 source for 7 days following the testing principles of the OECD test guideline 221. A suite of bioassays was applied to assess the biological effects of gamma radiation at multiple levels of biological organization, including detection of reactive oxygen species (ROS), oxidative stress responses (total glutathione, tGSH; lipid peroxidation, LPO), DNA damage, mitochondrial dysfunctions (mitochondrial membrane potential, MMP), photosynthetic parameters (chlorophyll *a*, chl *a*; chlorophyll *b*, chl *b*; carotenoids; Photosystem II (PSII) performance; CO_2 uptake), intercellular signaling (Ca^{2+} release) and growth. Gamma radiation increased DNA damage, tGSH level and Ca^{2+} content together with reduction in chlorophyll content, maximal PSII efficiency and CO_2 uptake at dose rates between 1 and 14 mGy/h, whereas increases in cellular ROS and LPO, inhibition of MMP and growth were observed at higher dose rates (≥24 mGy/h). A network of toxicity pathways was

* Corresponding authors at: Norwegian Institute for Water Research (NIVA), Section of Ecotoxicology and Risk Assessment, Gaustadalléen 21, N-0349 Oslo, Norway.
E-mail addresses: lix@niva.no (L. Xie), KET@niva.no (K.E. Tollefsen).

https://doi.org/10.1016/j.scitotenv.2019.05.016

proposed to portray the causal relationships between gamma radiation-induced physiological responses and adverse outcomes to support the development of Adverse Outcome Pathways (AOPs) for ionizing radiation-mediated effects in primary producers.

1. Introduction

There are multiple forms of ionizing radiation, including radioactive particles (alpha, beta, and neutrons) and electromagnetic waves (gamma and X-ray radiation). In general, as much as 80% of the external background radiation in the environment is generated from Naturally Occurring Radioactive Materials, NORM (Ramachandran, 2011), whereas use of radionuclides in nuclear energy, medical industries, Technologically Enhanced Naturally Occurring Radioactive Material (TENORM) from different sources also contribute to the total exposure to ionizing radiation (Miller and Miller, 2016; Nair et al., 2014). Among the different ionizing radiation types, gamma radiation is one of the most studied due to due to its relevance as an important dose contributor to both man and biota and the relative ease of performing external gamma exposure and dosimetry under well-defined, controlled conditions (Lind et al., 2019).

Due to public and environmental safety issues, the harmful effects of gamma radiation have been investigated in different organisms from terrestrial higher plant to crustacean, fish and mammals (Kovacs and Keresztes, 2002; Real et al., 2004; Gilbin et al., 2008; Vanhoudt et al., 2010). It is well established that gamma radiation can induce a range of abnormalities in biological systems if the dose rates and total doses are high enough (Reisz et al., 2014). For instance, plants and animals living in the Exclusion Zone in Chernobyl and Fukushima suffered acute adverse effects including increased mortality, reproduction inhibition and morphological changes (Geras'kin et al., 2008; Hiyama et al., 2012; Møller et al., 2013). Aquatic plants exhibit key roles in the ecosystems as primary producers, but also provide shelter and nutrition that sustains important functions for the rest of the ecosystem (Thormar et al., 2016). Compare to terrestrial non-human biota, aquatic plants may be subject to significant exposure to radiation in case of accidental discharges of radionuclides to their aquatic habitat (Kryshev and Sazykina, 1998; Wada et al., 2016).

Studies have indicated that gamma radiation may affect the growth of plants through induction of genomic, biochemical, physiological and morphogenetic changes in cells and tissues (Geras'kin, 2016). One of the initial events is direct energy dissipation and damage to biological macromolecules, such as DNA by introducing single and double strand breaks that can induce cell apoptosis and affect cellular functional responses leading to growth inhibition (González et al., 2012; Manova and Gruszka, 2015). Radiation also acts indirectly to form reactive oxygen species (ROS) in organisms through radiolysis of water (LaVerne, 2000). When the antioxidant capacity becomes exhausted, increase in ROS is expected to induce oxidative stress that can trigger biochemical and physiological processes in cells to ultimately inhibit growth (Hameed et al., 2008). Depending on the dose of gamma radiation, the excessive ROS produced has been demonstrated to directly induce lipid damage (Hameed et al., 2008), modulate the antioxidant systems (Wi et al., 2007), and impact various physiological response such as mitochondrial functions (Kovacs and Keresztes, 2002) in plants. Moreover, effects of gamma radiation on photosynthetic activity have been also presented in different studies (McCabe et al., 1979; Gomes et al., 2017). However, the mechanism about gamma radiation-mediated photosynthetic responses is still unclear. Additionally, cross-talk between ROS and cellular signaling systems as a response to stressors is increasingly becoming recognized to play key cellular and functional roles in plants (Aldon et al., 2018; Mazars et al., 2010). Although the number of studies documenting effects is steady increasing, only a few studies have systematically documented the linkage between the MoAs and adverse effects of ionizing radiation in primary producers.

In the present study, duckweed *Lemna minor* was chosen as a model to better understand the effects of gamma radiation on a representative aquatic plant. As a primary producer, *L. minor* harvests energy from solar light through photosynthesis to generate carbohydrates and oxygen through photosynthesis, and it is an important food source for fish and birds (Landolt and Kandeler, 1987). Due to its rapid reproduction rate in limited space and ease of maintenance under laboratory conditions, *L. minor* has become a popular test species for various environmental stressors, including studies with ionizing radiation (Bowen et al., 1962; Van Hoeck et al., 2015). We hypothesized that gamma radiation enhance oxidative stress and DNA damage as the main molecular MoA, which will collectively perturb a number of physiological mechanisms that ultimately lead to growth inhibition as an adverse outcome at the organism level in *L. minor*. To evaluate the hypothesis, the present study aimed to identify the causal links between MoA and adversity of ionizing radiation from a cobalt-60 (^{60}Co) source as a prototypical stressor by characterizing changes to ROS production, intracellular concentration of the antioxidant glutathione (GSH), LPO formation, DNA damage, MMP, photosynthesis (photosystem II (PSII) performance, CO_2 uptake), pigment content (Chl *a*, *b* and total carotenoids) and intercellular Ca^{2+}. The findings were assembled into dose rate-dependent toxicity pathways to aid establishing data-aggregation and data-mining frameworks such as Adverse Outcome Pathways (AOPs) for ionizing radiation in primary producers.

2. Materials and methods

2.1. Culture and gamma radiation exposure

Lemna minor used in this study was obtained from Ghent University, Belgium and registered in the Rutgers Duckweed stock cooperative (Strain ID: 5544). The stock culture of duckweed fronds was maintained in glass aquariums, which were placed in a climate-controlled room at 24 ± 2 °C with 16 h light/8 h dark irradiation (80 ± 5 μmol photons m^{-2} s^{-1}) for three weeks prior to the experiments. The culture medium was SIS medium (OECD, 2006) containing 85 mg/L $NaNO_3$, 36 mg/L $CaCl_2.2H_2O$, 90 mg/L KH_2PO_4, 75 mg/L, $MgSO_4.7H_2O$, 1 mg/L H_3BO_3, 0.05 mg/L $ZnSO_4.7H_2O$, 0.01 mg/L $Na_2MoO_4.2H_2O$, 0.2 mg/L $MnCl_2.4H_2O$, 0.84 mg/L $FeCl_3.6H_2O$, 0.01 mg/L $Co(NO_3)_2.6H_2O$, 0.005 mg/L $CuSO_4.5H_2O$ and 1.4 mg/L EDTA disodium-dihydrate. The pH of the test solutions was 6.5 ± 0.2 during the test.

Gamma radiation exposures were conducted at the FIGARO experimental facility at the Norwegian University of Life Sciences in Ås, Norway (Lind et al., 2019). *Lemna minor* was exposed for a total of 7 days to external ^{60}Co gamma (^{60}Co; 1173.2 and 1332.5 keV γ-rays) in 6-well, clear polystyrene microplate (Corning® BioCoat™, New York, USA), five gamma dose rates combined with a control were run at low dose rate (1–46 mGy/h, n = 6) and one high dose rate (70 mGy/h, n = 4). Dose rates were selected according to the results from previous studies and literatures to capture complete dose rate-effect relationships encompass (Harrison and Anderson, 1996; Hevrøy et al., 2019; Hochmal et al., 2015), whenever possible. The exposure was repeated three times under the same conditions. For the exposure experiments, microplates were positioned at different distances away from the gamma radiation source corresponding to the dose rates to water (D_{Water}) (Fig. 1 and Supplementary Table S1). The dosimetry

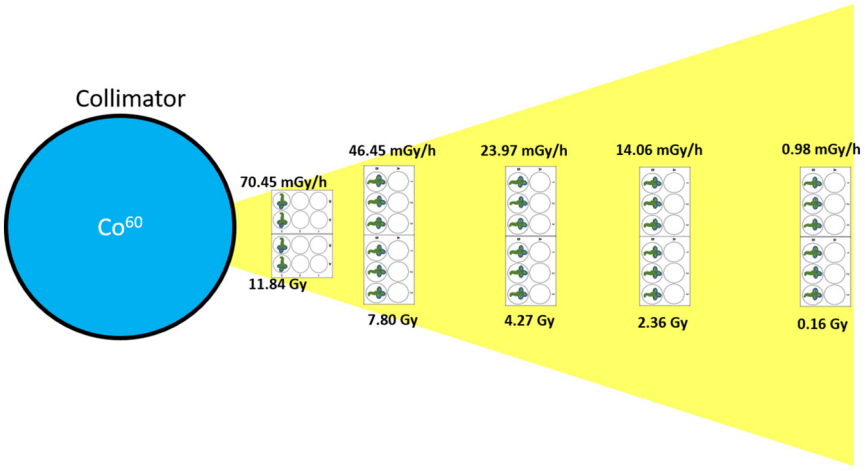

Fig. 1. The dose rates (top) and total dose (bottom) used in the gamma radiation exposures with *Lemna minor*.

was traceable to the Norwegian Secondary Standard Dosimetry Laboratory (Norwegian Radiation and Nuclear Safety Authority, DSA, Oslo, Norway). Dose rates to water in the center of the 6-well plates were estimated according to Bjerke and Hetland (2014) and used as a proxy for the dose rates to *L. minor*. Actual dose rates were measured by Optically Stimulated Luminescence (OSL) based dosimetry system using nanoDots dosimeters and InLight microSTAR reader (Landauer®, Velizy-Villacoublay Cedex, France). Nanodots with 5 mm polypropylene build-up caps were exposed in the middle of the 6-well plates to represent the average dose rate (mGy/h) and calculate the total dose (mGy) after 7 days of exposure.

2.2. Growth inhibition

The growth rate parameters, frond number, frond size and fresh weight were analyzed essentially as described in the OECD TG221 (OECD, 2006). The frond area was calculated based on the whole-plant imaging with a floating scale bar by a digital camera (FinePix S2500HD, Fujifilm, Japan). The frond area in each photograph was analyzed using the Image-J software program version 1.48 (National Institutes of Health, Maryland, USA). The fresh weight was measured by weighing all material including fronds and root from one well after drying excessive fluid by a dry lint-free paper tissue.

2.3. Oxidative stress bioassays

2.3.1. ROS formation

Direct intracellular ROS production was determined by a fluorescent probe down-scaled into a 96 well format, essentially as described by Razinger et al. (2010). The fluorescent probe 2,7-Dichlorodihydrofluorescein diacetate (H_2DCFDA) (Invitrogen Molecular Probe, Eugene, Oregon, USA) was used to determine the ROS formation in *L. minor*. A 50 mM H_2DCFDA stock solution was prepared in dimethyl sulfoxide (DMSO) (Purity 99.7%; Sigma-Aldrich, St-Louis, MO, USA) and stored at −20 °C until use. The stock solution was dissolved in the SIS medium to reach a final working concentration of 50 μM. Two 200 μl of working solution was transferred to each well of a 96-well microplate (Corning Incorporated, Costar®, NY, USA) containing one *L. minor* with 3 fronds. The fluorescence was recorded after 1 h probe loading using a VICTOR^3 plate reader, 1400 Multilabel Counter (Perkin Elmer, Massachusetts, USA) with excitation at 488 nm and emission at 520 nm. The relative fluorescence obtained was normalized by fronds weight and expressed as fold change compared to the control.

2.3.2. Measurement of lipid peroxidation

The oxyl and peroxyl radicals associated with lipid peroxidation (LPO) was measured in *L. minor* fronds by the fluorescent dye C11-BODIPY$^{581/591}$ (Invitrogen Molecular Probe, Eugene, Oregon, USA) as originally described by Cheloni and Slaveykova (2013) with minor modifications by Almeida et al. (2017). BODIPY is a fatty acid analogue with specific fluorescence properties which can be subject to oxidation by oxyl-radicals together with endogenous fatty acids inside the cellular membrane and thus acts as an indicator of potential LPO (Cheloni and Slaveykova, 2013). Stock solutions of 5 mM were prepared in DMSO and stored at −20 °C until use. The stock solution was dissolved in SIS medium to reach a final concentration of 10 μM working solution and then transferred 200 μl into each well of 96-well microplate containing one exposed colony with 3 fronds. After 1 h staining, fronds were washed by medium and the fluorescence quantified by a Victor 3 plate reader at excitation/emission wavelength of 488/535 nm. The relative fluorescence obtained was normalized by fronds weight and expressed as fold change compared to the control.

2.3.3. Total glutathione (tGSH) levels

The total GSH (tGSH) content was determined using the non-fluorescent cell-permeant probe monochloramine (mBCI) as described elsewhere (Machado and Soares, 2012; Almeida et al., 2017). This probe reacts with intracellular GSH by forming the fluorescent bimane-glutathione (B-SG) adducts through glutathione S-transferase (GST) catalyzation (Haugland, 2005). In brief, a stock solution of 5 mM mBCI (Invitrogen Molecular Probe, Eugene, Oregon, USA) in DMSO and 10 U/ml GST in assay buffer (Sigma-Aldrich, United Kingdom) were prepared and stored at −20 °C until use. Before staining, 200 μl stock mBCI solution and 2000 μl GST were added to the SIS media to achieve a 50 μM (1 U/ml) working solution. After exposure, one exposed colony together with 200 μl working solution were transferred into the well of 96-well microplate and incubated in the dark for 1 h with orbital shaking. The fluorescence of the probe was recorded by a VICTOR^3 plate reader set to excitation at 405 nm and emission at 488 nm after rinsing the fronds with fresh medium. The relative fluorescence obtained was normalized by fronds weight and expressed as fold change compared to the control.

2.4. Comet assay

Genotoxicity was assessed by the alkaline version of the comet assay (Single Cell Gel Electrophoresis) as described by Gichner et al. (2004), with minor modifications. Briefly, 20 fronds were placed in a Petri dish containing 400 μl of ice-cold extraction buffer (PBS + EDTA) and

cut into small pieces with a sterile razor blade to isolate the nuclei. 75 μl of nuclei solution was gently mixed with 50 μl 1% (w/v) low melting point agarose (Invitrogen, Eugene, OR, USA) and the mixture was molded into agarose-coated glass slides (Sigma-Aldrich, Oslo, Norway). Prior to electrophoresis, the slides were placed in an electrophoresis buffer (1 mM EDTA and 300 mM NaOH, pH > 13) for 15 min at 4 °C to allow the DNA to unwind. Following denaturation, electrophoresis was performed in the same buffer and in the same conditions at 0.72 V cm^{-1} and 300 mA for 5 min. After electrophoresis, slides were gently placed into dH20 for 1 min and then rinsed 3 times with neutralization buffer (400 mM Tris buffer, pH 7.5). The gels were then fixed with ethanol (95%) for dehydration and dried overnight. To analyses the DNA damage, slides were stained with 1.5 ml of diluted SYBR Gold (1/5000) (Life Technologies Ltd., Paisley, UK; dilution 1:5000) for 20 min and then washed 3 times with dH_2O to remove the excess of SYBR Gold. Fifty randomly chosen nuclei per replicate were analyzed under a microscope Olympus IX71 with a CCD camera (Olympus, Tokyo, Japan) equipped with a high-intensity fluorescence illumination system (X-city 120, Excelitas Technologies Crops., Fremont, Canada). The computerized image analysis system OpenComet v1.3.1 was used to measure the tail DNA (% tail DNA = 100 − % head DNA) for the quantification of DNA damage (Gyori et al., 2014).

2.5. Mitochondrial oxidative phosphorylation

The mitochondrial inner membrane potential (MMP) was measured as a proxy for the uncoupling of mitochondrial oxidative phosphorylation (OXPHOS) using tetramethylrhodamine methyl ester (TMRM, Invitrogen Molecular Probe, Eugene, Oregon, USA) following the method of Ehrenberg et al. (1988) and Scaduto and Grotyohann (1999), with minor modifications for use with plants and algae (Jamers et al., 2009). In brief, stock solutions of TMRM (5 mM) were prepared in DMSO and stored in the dark at −20 °C until use. Before staining, 2 μl TMRM stock solution was added into SIS medium to achieve 500 nM working solution. After exposure, one *L. minor* colony with 3 fronds were transferred into the well. The fronds were incubated with TMRM in the dark (2 h, room temperature), fronds were rinsed with SIS medium for 5 min to remove free (unbound) TMRM and transferred 200 μl SIS medium in 96-well black clear-bottom microplates. The fluorescent intensity of TMRM was measured using VICTOR^3, 1400 Multilabel Counter using the excitation wavelength of 530 nm and the emission wavelength of 590 nm. The relative fluorescence obtained was normalized by fronds weight and expressed as percentage compared to the control.

2.6. Determination of photosynthetic pigment content

Pigment content was determined spectrophotometrically, essentially as described by Lichtenthaler and Buschmann (2001). In brief, 50 mg of whole plants tissue (wet weight) included fronds and roots were collected and homogenized in methanol (Purity: 99.9%, Sigma-Aldrich, Oslo, Norway) for 30 min, the solution centrifuged at 3000 rpm (10 min) and the absorbance at 652, 665, 470 and 470 nm determined by a UV–vis spectrophotometer (Perkin-Elmer, Lamdba 40, Akron, Ohio, USA) as detailed in Xie et al. (2018). Chlorophylls content (chlorophyll *a* and *b*) and total carotenoids content were calculated according to equations by Lichtenthaler (1987). Results were normalized to fresh weight and expressed as percentage reduction compare to control.

2.7. Chlorophyll a fluorescence

Pulse-Amplitude-Modulated (PAM) chlorophyll fluorescence kinetics was measured simultaneously for all samples by a PAM 2000 fluorometer (Walz, Effeltrich, Germany) as described by Hulsen et al. (2002). In brief, the *L. minor* fronds were dark-adapted 30 min before each measurement. Basal fluorescence (F_o) was measured under weak modulated illumination (1 μmol m^{-2} s^{-1}). The maximum fluorescence (F_m) was obtained by applying a saturating light pulse (5000 μmol m^{-2} s^{-1}, 0.8 s). The light-adapted fluorescence parameters such as effective minimal fluorescence (F_o') and steady-state terminal fluorescence (F_t) were measured after 30 min of continuous illumination of 80 μmol m^{-2} s^{-1} from a high intensity LED panel (Model SL-3500, Photon System Instruments, Brno, Czech Republic). Light adapted maximal fluorescence (F_m') was obtained by applying a saturating light pulse. All the values determined during the measurement (F_o, F_o' F_m, F_m' and F_t) allowed the calculation the maximum quantum yield of photosystem (F_v/F_m) and operating efficiency of PSII ($\Phi_{PSII} = (F_m'-F_t)/F_m'$). The Photochemical parameters were calculated as described by Baker (2008). Non-photochemical quenching (NPQ) and photochemical quenching (qP) was calculated using equations (NPQ = (Fm-Fm′)/Fm′ and qP = (Fm′-Ft)/ (Fm-Fo′)). Results were expressed as percentage reduction compare to control.

2.8. CO_2 uptake

CO_2 uptake was detected by using an infrared gas-exchange system. In brief, around 20 individual *L. minor* colonies were collected into a 55 mm petri dish (VWR, Oslo, Norway) containing 5 ml SIS medium. The petri dish was placed into Bryophytes chamber (6400-24 LI-COR, Inc., Lincoln, NE, USA) with an RGB light Source (model 6400-18 , Inc., Lincoln, NE, USA) connected to a portable CO_2 analyzer (model LI-6400XT LI-COR, Inc., Lincoln, NE, USA). The CO_2 uptake measurements were performed with a CO_2 concentration of 400 μmol mol^{-1}, a temperature of 24 °C and a photon flux density of 100 μmol m^{-2} s^- with equal levels of red, green and blue light. The net CO_2 uptake was normalized to total frond size automatically and presented as percentage reduction compared to the control group.

2.9. Determination of intracellular calcium

Fluo-3 acetoxymethylester (Fluo-3/AM) (Invitrogen Molecular Probe, Eugene, Oregon, USA) was used to characterize the intracellular Ca^{2+} level, essentially as described by Li et al. (2014). In brief, a stock solution of 5 mM Fluo-3/AM was prepared in DMSO (Purity 99.7%, Sigma-Aldrich), 2 μl Fluo-3 of the solution was added into SIS medium to achieve a 500 nM working solution and 200 μl working solution was transferred to each well of 96-well microplate. After 1 h staining in darkness at 4 °C, fronds were rinsed and placed into a new microplate with 200 μl clean SIS medium and the fluorescent intensity was measured by the microplate reader VICTOR^3 plate reader with the wavelength 488/520 (excitation/emission). The fluorescence of the exposure media in combination with the dye (without the presence of fronds) was also analyzed and the resulting fluorescence subtracted. The relative fluorescence obtained was normalized by fronds weight and expressed as percentage induction compared to the control.

2.10. Data treatment and statistical analysis

All statistical and graphical analysis were conducted in GraphPad Prism version 6 (GraphPad Software, La Jolla, California, USA). The results are presented as the mean replicates ± standard error. Shapiro-Wilk and Levene's tests were applied to test normality and homogeneity of variances, respectively. Differences between controls and treated samples were analyzed by one-way ANOVA followed by Dunnett's multiple comparison test using a threshold of $p < 0.05$ for significance to characterize the No Effect Dose rate (NOEDR) and Lowest Effect Dose rate (LOEDR). Non-linear regression was used to estimate the dose-response relationships from zero to 100% to estimate the dose rate causing 10% and 50% Effect Dose Rate (EDR_{10} and EDR_{50}). A principal component analysis (PCA) was applied to the full data set to characterize relationships between endpoints using XLSTAT2018 (Addinsoft, Paris,

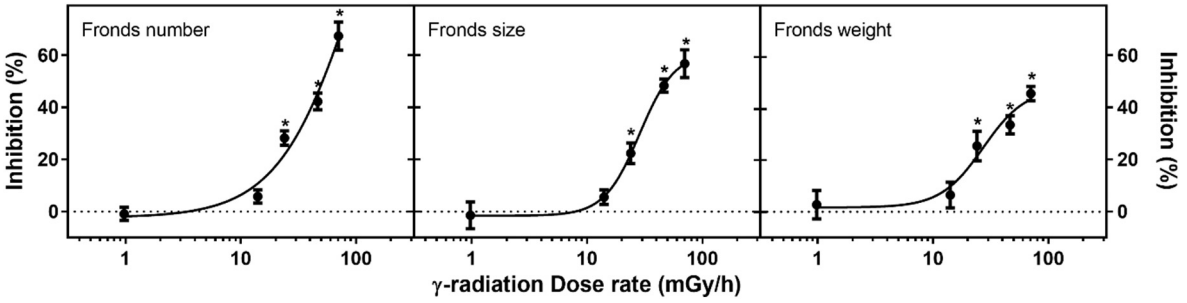

Fig. 2. Growth inhibition measured as (A) frond number (FN), (B) frond size (FS) and (C) fresh weight (FW) in *Lemna minor* exposed to gamma radiation for 7 days (Mean ± SEM). Dotted line indicates the control level and the solid line shows the fitted non-linear regression curve, whereas the asterisk (*) indicates significant differences compare to the control.

France). The same software was used to calculate Pearson's correlation coefficients as an estimate of the strength of association between the different endpoints ($p < 0.05$).

3. Results

3.1. Growth inhibition

After 7 days exposures, gamma radiation caused a dose rate-dependent reduction in *L. minor* growth. As much as 70% inhibition in frond number (FN), 60% inhibition on frond size (FS) and 50% inhibition in frond fresh weight (FW) was observed at 70 mGy/h (Fig. 2). Estimated EDR_{50} for FN, FS and FW ranged between 32 and 125 mGy/h, whereas NOEDR and LOEDR ranged between 14 and 24 mGy/h for the different growth parameters, respectively (Table 1).

3.2. Oxidative stress (ROS and tGSH)

A dose rate-dependent response relationship was observed in oxidative stress parameters after 7 days of exposure (Fig. 3). Both cellular ROS formation and LPO increased 2.5-fold at 70 mGy/h compared to control (Figs. 3A and 4B), whereas maximal induction of tGSH occurred at 46 mGy/h (Fig. 3C). The NOEDR and LOEDR ranged between 14 and 23 mGy/h for cellular ROS and LPO formation, respectively (Table 1). The tGSH induction was higher than controls at the lowest dose-rate and therefore yielded a NOEDR and LOEDR of <1 mGy/h and 1 mGy/h, respectively (Table 1).

3.3. Lipid peroxidation (LPO) and DNA damage

Lipid peroxidation (LPO) induced by increased gamma radiation dose rates was observed after 7 days of exposure (Fig. 3C). At 70 mGy/h, lipid peroxidation increased over 2-fold compared to control. The Comets assay result presented a dose rate-dependent DNA damage (percent of tail DNA) after exposed to gamma radiation. Maximum DNA damage occurred at 70 mGy/h (Fig. 4). The EDR_{50} for DNA damage was predicted to occur at fairly high dose rates (146 mGy/h). Both LPO and DNA damage had NOEDR and LOEDR ranged between 14 and 24 mGy/h, respectively (Table 1).

3.4. Mitochondrial inner membrane potential

The MMP was reduced in a dose rate dependent manner after exposure for 7 days. At the highest dose rate of 70 mGy/h MMP was reduced as much as 40% (Fig. 5A). The 7 day EDR_{50} of MMP was estimated to be 145 mGy/h, whereas the NOEDR and LOEDR for MMP ranged between 14 and 24 mGy/h, respectively (Table 1).

3.5. Intracellular Ca^{2+} level

A dose rate-dependent increase in intracellular Ca^{2+} accumulation was observed after exposed to gamma radiation. Intracellular Ca^{2+} level increased as much as 60% at 70 mGy/h (Fig. 5B). The EDR_{50} of induction of Ca^{2+} was at 39 mGy/h, whereas NOEDR and LOEDR ranged between 1 and 14 mGy/h, respectively (Table 1).

Table 1
The estimated effective dose rate causing 10% and 50% effect (EDR_{10} and EDR_{50}) and lowest effect dose rate (LOEDR) in *L. minor* after 7 day exposed to gamma radiation. (Slope and regression coefficient (R^2) for nonlinear regression; not obtained (-), and not applicable (N/A).

Endpoints	EDR_{10} (mGy/h)	EDR_{50} (mGy/h)	NOEDR (mGy/h)	LOEDR (mGy/h)	Slope	R^2
FN	16.8	54.8 ± 13.5	14	24	1.7	0.958
FS	14.9	31.5 ± 7.1	14	24	2.9	0.978
FW	21.2	124.6 ± 53.8	14	24	1.3	0.912
F_v/F_m	28.9	156.3 ± 45.4	14	24	1.4	0.865
Φ_{PSII}	20.1	67.2 ± 13.1	24	46	1.8	0.921
qP	26.0	62.4 ± 26.4	14	24	2.5	0.964
NPQ	11.8	50.4 ± 8.3	14	24	1.5	0.873
CO_2 uptake	2.8	53.2 ± 11.4	1	14	0.8	0.950
Chl a	19.9	71.3 ± 25.8	1	14	1.7	0.931
Chl b	7.6	114.4 ± 2.13	1	14	0.8	0.920
Carotenoids	N/A	N/A	–	–	–	0.535
ROS	N/A	N/A	14	24	2.8	0.934
LPO	N/A	N/A	14	24	2.9	0.865
tGSH	N/A	N/A	–	1	4.6	0.711
MMP	21.8	144.7 ± 43.3	14	24	1.2	0.683
Ca^{2+} content	9.9	39.3 ± 24.41	1	14	1.6	0.862
DNA damage	19.45	164.2 ± 19.5	1	14	1.1	0.860

ROS–reactive oxygen species, GSH– Glutathione, LPO–lipid peroxidation, Ca^{2+}– Ca^{2+} concentration, qP–coefficient of photochemical quenching, NPQ–non-photochemical quenching, F_v/F_m–maximum quantum yield of PSII, Φ_{PSII}–operating efficiency of PSII, OXPHOS – oxidative phosphorylation, Fm–maximal fluorescence yield, ETR–electron transfer rate, Chl b–Chlorophyll a, Chl b–Chlorophyll b. FN-fronds number, FS-frond size, FW-frond fresh weight.

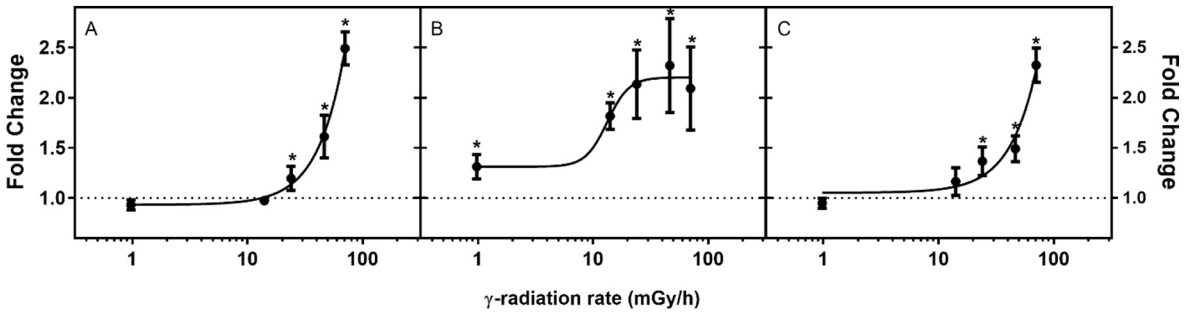

Fig. 3. Change in oxidative stress determined as (A) ROS formation, (B) total Glutathione (tGSH) and (C) lipid peroxidation (LPO) in *Lemna minor* after 7 days' exposure to different dose rates of gamma radiation. Dotted line indicates the control level and the solid line shows the fitted non-linear regression curve, whereas the asterisk (*) indicates significant differences compare to the control.

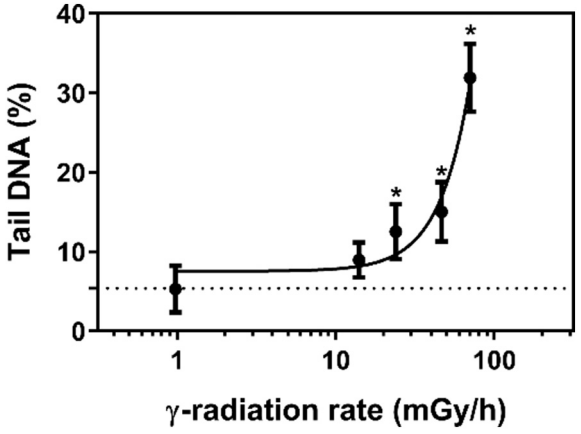

Fig. 4. DNA damage in *Lemna minor* after 7 days exposure to different dose rates of gamma radiation measured as tail DNA by the Comet assay. Dotted line indicates the control level and the solid line shows the fitted Non-linear Model through the data. The asterisk (*) indicate significant differences compare to the control at $P < 0.05$.

3.6. Pigments

Chl *a* and *b* concentration decreased in a dose rate dependent way after 7 days' exposure to gamma radiation. Maximal reduction of chlorophylls and total carotenoids content was at 70 mGy/h (Fig. 6A and B). Significant suppression of carotenoids content was observed at 24 mGy/h, with a maximum decrease of 20% at 70 mGy/h. The EDR_{50} of chlorophylls were typically between 71 and 114 mGy/h, and the NOEDR and LOEDR ranged between 1 and 14 mGy/h, respectively (Table 1). No NOEDR and LOEDR for carotenoids were detected in this study (Fig. 6C and Table 1).

3.7. Inhibition of photosynthesis and PSII performance

Photosynthetic CO_2 uptake decreased with increasing dose rate after 7 days' exposure to gamma radiation, and 70 mGy/h caused as much as a 60% reduction in CO_2 uptake (Fig. 7). Estimated EDR_{50} was 53.2 mGy/h, whereas the NOEDR and LOEDR were 1 mGy/h and 14 mGy/h, respectively (Table 1). Of the PSII parameters measured, F_v/

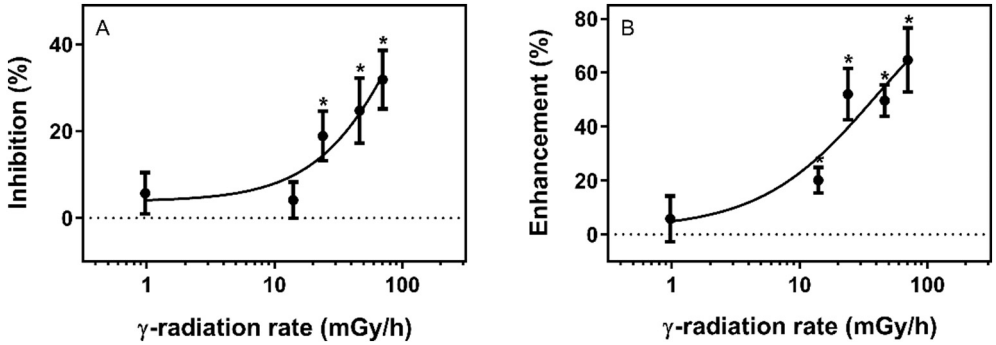

Fig. 5. (A)Mitochondrial inner membrane potential (MMP) and (B) intracellular calcium level in *Lemna minor* after 7 days' exposure to different dose rates of gamma radiation: Dotted line indicates the control level and the solid line shows the fitted Non-linear Model through the data. The asterisk (*) indicate significant difference compare to the control at $P < 0.05$.

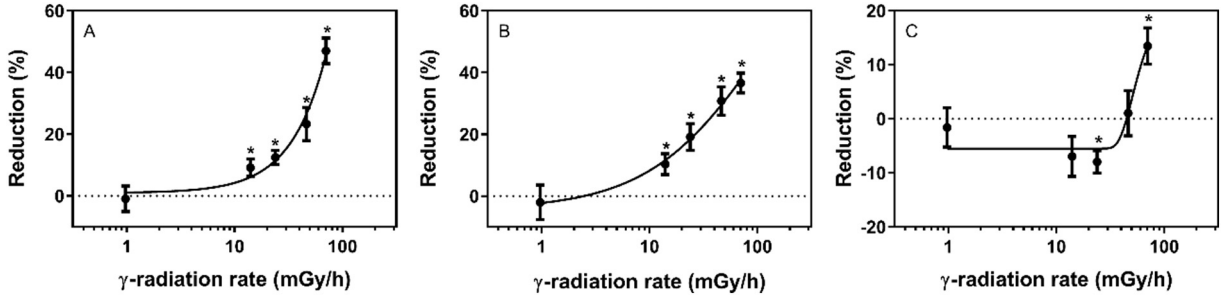

Fig. 6. Reduction in pigment content as (A) chlorophyll *a* (Chl *a*), (B) chlorophyll *b* (Chl *b*), (C) total carotenoids in *Lemna minor* after 7 days' exposure to different dose rates of gamma radiation. Dotted line indicates the control level and the solid line shows the fitted Non-linear Model through the data. The asterisk (*) indicated significant difference compare to control at $P < 0.05$.

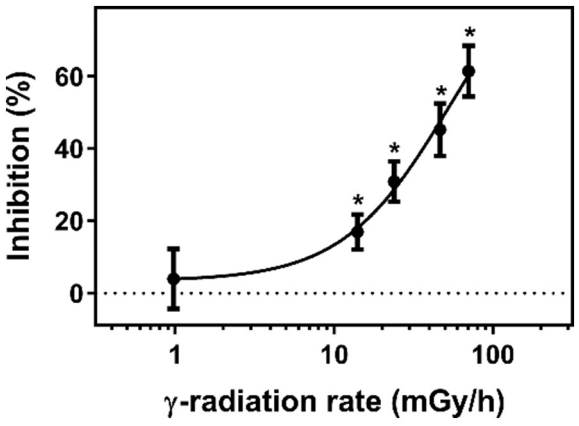

Fig. 7. Inhibition of net photosynthetic CO_2 uptake in *Lemna minor* after 7 days of exposure to different dose rates of gamma radiation. Dotted line indicates the control level and the solid line shows the fitted Non-linear Model. The asterisk (*) indicated significant difference at $P < 0.05$.

F_m and Φ_{PSII} decreased 40% and 50%, while NPQ and qP decreased over 60% at the highest dose rates (Fig. 8). Estimated EDR_{50} of F_v/F_m, Φ_{PSII}, qP and NPQ were 156.3 mGy/h, 67.5 mGy/h, 62.4 mGy/h and 50.4 mGy/h, respectively. The LOEDR for Φ_{PSII} were 24 mGy/h while the 3 other parameters displayed a LOEDR of 14 mGy/h (Table 1).

3.8. Principle component analysis

The two principal components (PC1 and PC2) explained as much as 89.4% of total variance (Fig. 9). All the variables related to the PC1 showed a clear separation between the low and high gamma dose rates, which explained 89.41% of total variance. For the PC1, the growth reduction (FN, FA and FW), PSII parameters (F_v/F_m, Φ_{PSII} and qP), and pigments content were all associated with low gamma radiation dose rates (0, 1 and 14 mGy/h). However, the correlation between exposure and ROS formation, LPO and DNA damage were associated with the higher gamma radiation dose rates (24, 46 and 70 mGy/h). Pearson correlation analysis (Supplementary Table S2) demonstrated that the inhibition of growth (FN, FA and FW), inhibition of PSII efficiency and reduction of net photosynthesis (CO_2 uptake) and MMP were positively correlated, but inhibition of growth was negatively correlated with induction of oxidative stress (ROS and tGSH) and damage (LPO and DNA damage) (Supplement Table 1). The PC2 only explained 8.2% of total variance, two main groups separated by PC2 were tGSH and Ca^{2+} from DNA damage, LPO and ROS.

4. Discussion

This study aimed at providing mechanistic insight into how gamma radiation affected key processes at the cellular or organ level, and how these perturbations led to inhibition of growth and reproduction in the aquatic primary producer *L. minor*. In the present study, we determined the effects of gamma radiation on ROS formation, oxidative damage (LPO), DNA damage, uncoupling of OXPHOS, photosynthesis (CO_2-uptake, PSII parameters including F_v/F_m, Φ_{PSII}, NPQ, qP), antioxidant (tGSH), pigments (Chl *a*, Chl *b* and total carotenoids) and Ca^{2+} content, and how these parameters were associated with changes in frond development and reproduction. The results from the presented study clearly demonstrated that gamma radiation caused a number of physiological changes that were dose rate-dependent. The different results are presented in subsequent sections to characterize the potential causal relationships between MoAs and adversity (Fig. 10).

4.1. Growth inhibition

Gamma radiation had a negative impact on *L. minor* growth assessed by three different, but related endpoints including frond number, frond size and frond weight (Table 1). Although a dose rate-dependent inhibition was observed in all three growth endpoints, the EDR_{50} data suggested that FN was less sensitive than FW and FS, and indication that inhibition of fronds development (size and weight) occurred before reproduction (e.g. FN). Inhibition of frond size and weight can be caused by the reduction of frond cells number and volume as consequences of the interaction of senescence-rejuvenation cycles (Severi and Fornasiero, 1983). The current growth responses on *L. minor* were found to be more sensitive than Van Hoeck's study et al. (2015), which may indicate that different exposure systems included strains, medium compositions, light conditions, and pH may also influence the

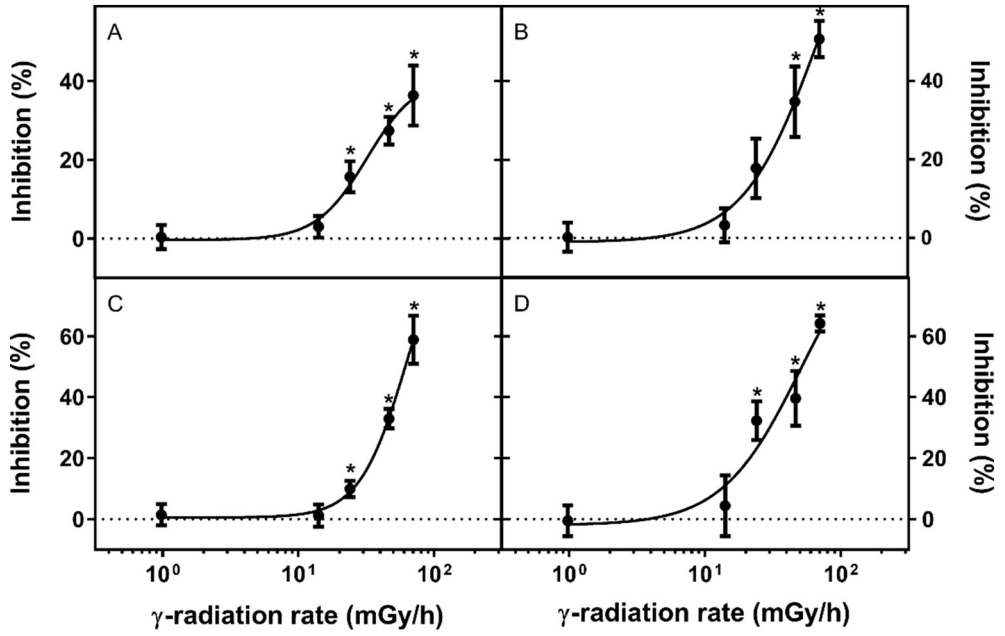

Fig. 8. Inhibition of photosystem II performance as (A) maximal PSII efficiency (F_v/F_m), (B) operating efficiency of PSII (Φ_{PSII}) (C) photochemical quenching (qP) and (D) non-photochemical quenching (NPQ) in *Lemna minor* after 7 days of exposure to different dose rates of gamma radiation. Dotted line indicates the control level and the solid line shows the fitted Non-linear Model through the data. The asterisk (*) indicated significant difference compare to control at $P < 0.05$.

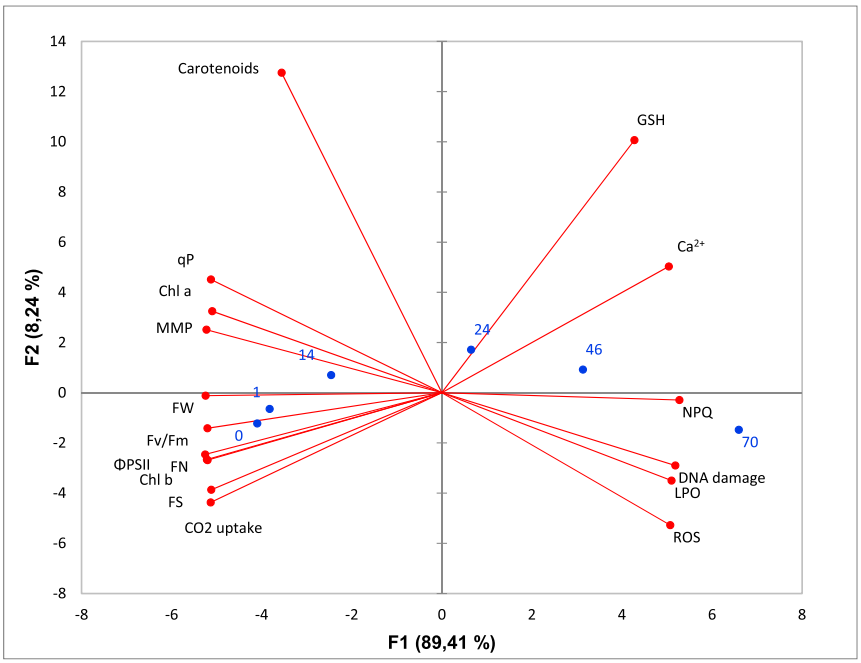

Fig. 9. Principal component analysis (PCA) of responses in *Lemna minor* exposed to gamma radiation for 7 days. ROS–reactive oxygen species, GSH– Glutathione, LPO–lipid peroxidation, Ca^{2+}–Ca^{2+} concentration, qP–coefficient of photochemical quenching, NPQ–non-photochemical quenching, F_v/F_m–maximum quantum yield of PSII, Φ_{PSII}–operating efficiency of PSII, MMP – mitochondrial inner membrane potential, ETR–electron transfer rate, Chl b–Chlorophyll a, Chl b–Chlorophyll b, FN-fronds number, FS-frond size, and FW-frond f weight. Blue number denotes the dose rates.

overall sensitivity of *L. minor* to stressors (Hodgson, 1970; McLay, 1976; Vidaković Cifrek et al., 2013). Interestingly, Species Sensitivity Distributions (SSD) data for 9 terrestrial plants (Garnier-Laplace et al., 2013) suggest that the EDR_{10} for the growth endpoints in *L. minor* (15–21 mGy/h) is much lower than *Hordeum* sp., *Fagopyrum esculentum* and *Triticum monococcum*, and confirm that *L. minor* is susceptible to external gamma radiation.

4.2. Oxidative stress

4.2.1. Generation of ROS and depletion of tGSH

The present study demonstrated that exposure to gamma radiation dose rates above 24 mGy/h significantly enhanced cellular ROS production in *L. minor*. After exposure, radiolysis can directly generate ROS including hydroxyl radicals (·OH), superoxide anion ($O_2^{\cdot-}$), hydrogen peroxide (H_2O_2), and singlet oxygen ($^1O_2$) production in plants (Tripathy and Oelmüller, 2012). Beside radiolysis, endogenous ROS are usually produced as a consequence of aerobic metabolic processes in plants, such as photosynthesis and respiration (Reisz et al., 2014). In the chloroplasts, the reaction centres of PSI and PSII are the major sites for ROS formation (Asada, 2006). ROS such as H_2O_2 is mainly generated in PSI by the Mehler's reaction (Mehler, 1951), whereas triplet state oxygen ($^3O_2$) is excited to singlet oxygen ($^1O_2$) by the triplet excited state chlorophyll ($^3Chl^*$) as the major ROS in PSII (Tripathy and Oelmüller, 2012). However, the reduction of electron transport chain components can also enhance the formation of $^1O_2$ through induction

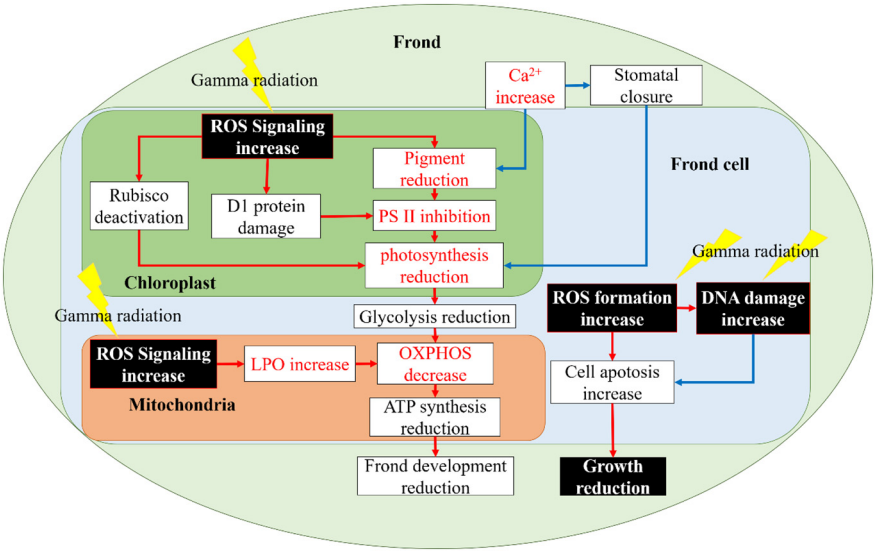

Fig. 10. Proposed toxicity pathway network for ionizing radiation induced growth inhibition in primary producers. Blue arrow indicated the low dose rate effect (1, 14 mGy/h) and the red arrow indicate the high dose rate (24, 46, 70 mGy/h) effects marked endpoints were detected in this study while white marked endpoints were included based on literatures. Endpoints measured in this study were marked in red text.

of superoxide radicals' formation (Kozuleva and Ivanov, 2016). Such an increase in mitochondrial ROS formation may induce cell damage through a series of events involving O_2^- interaction with protein iron–sulfur (Fe—S) clusters that induce generation of highly reactive hydroxyl radicals (•OH) by the Fenton reaction (Liochev and Fridovich, 1994) and ultimately damage mitochondrial lipids (Martínez-Reyes and Cuezva, 2014).

In plant cells, the ROS level is regulated by ROS scavenging pathways involving enzymatic and non-enzymatic antioxidants (Choudhury et al., 2013). Normally, the radicals formed by ionizing radiation will be rapidly eliminated by the antioxidant defence mechanisms (Reisz et al., 2014). In this study, induction of the antioxidant tGSH was identified to be the most sensitive response to gamma radiation (LOEDR = 1 mGy/h), thus suggesting that inducible cellular non-enzymatic antioxidants are key to the cellular defence against ROS-associated damage at low dose rates. In general, GSH is an essential metabolite with multiple functions in plants (Greenberg and Demple, 1986) and has been proposed to protect cells from oxidative damage such as that formed by ionizing radiations-induced H_2O_2 (Noctor et al., 2012). Interestingly, lack of a strong correlation between GSH and ROS formation (≤0.95) indicate that other antioxidant defence systems might also be involved in the protection against ROS-associated damage in *L. minor*. For example, superoxide dismutase (SOD), being responsible for the conversion of O_2^- to H_2O_2, was the most sensitive antioxidant enzyme defence response determined in *L. minor* when exposed to gamma radiation (Van Hoeck et al., 2015). It's therefore likely that *L. minor* maintains a highly efficient ROS scavenging and inducible antioxidant enzymatic defence that limit direct ROS-induced damage at low dose rates.

4.2.2. DNA damage

Direct DNA damage through energy dissipation and oxidative damage is considered an important MoA for gamma radiation as well (Teoule, 1987; Imlay and Linn, 1988). In the present study, significantly increased DNA damage was observed from 14 mGy/h after exposed to gamma radiation. Elevated DNA damage at 14 mGy/h could be mainly due to the direct ionization by gamma radiation since no increase ROS formation was observed at this dose rate. However, induction of ROS was clearly correlated to DNA damage at higher dose rates to suggest adversity being linked to ROS-induced oxidative stress in *L. minor*. In plants, unrepaired DNA damage can potentially affect cellular functionalities by disturbing DNA replication and transcription, which can lead to the growth reduction (Manova and Gruszka, 2015).

4.2.3. Lipid peroxidation

When cellular ROS production exceeds the antioxidant capacity, ROS will cause damage to lipids (Najafi et al., 2014), and such damages are often localized close to the site of origin due to the high reactivity and short lifespan of many types of ROS (Asada, 2006). In plants, the membranes of chloroplast and mitochondria are likely the main targets for gamma-induced ROS through the production of lipid hydroperoxides (Shadyro et al., 2002). In the present study, significantly increased LPO was observed from 24 mGy/h and positively correlated to ROS formation. In addition, LPO was negatively associated with PSII efficiency and MMP, which suggested that LPO can potentially disturb the intracellular functions by perturbed the membrane bilayer or induced membrane degradation in both thylakoids and mitochondria (Halliwell, 1987; Ademowo et al., 2017).

4.3. Mitochondria membrane potential (MMP)

Oxidative phosphorylation (OXPHOS) produces ATP as a primary form of energy in aerobic organisms. Additionally, OXHPOS is also a source of ROS, as approximately 1–2% of oxygen consumed during physiological respiration is converted into superoxide when electrons prematurely leak from the electron transport chain (ETC) and are aberrantly transferred to molecular oxygen (Zorov et al., 2014). In this study, MMP was used as an indicator for uncoupling of OXPHOS and it was significantly inhibited at similar dose rates as many of the oxidative stress endpoints (LOEDR = 24 mGy/h). In general, MMP decreased indicated a reduction of ATP generation in mitochondria since MMP was an intermediate form of energy storage which is used by ATP synthase to make ATP (Zorova et al., 2018). The finding that reduction of MMP was correlated with the induction of ROS formation and LPO demonstrate that inhibition of MMP can be associated with oxidative damage to the mitochondrial membrane. Otherwise, ROS is also a key regulatory factor of the TCA cycle and OXPHOS in mitochondria (Liemburg-Apers et al., 2015). Moreover, ROS is proposed as well to trigger mitochondrial permeability transition pore (mPTP) formation in certain terrestrial plants (Panda et al., 2008) which may lead to loss of the electrochemical potential and uncoupling of OXPHOS.

4.4. Free intracellular calcium

Intracellular calcium ion (Ca^{2+}) is one of the most important secondary messengers involved in a number of signal transduction pathways in plants (Tuteja and Mahajan, 2007). The present study demonstrated that gamma radiation caused a dose rate-dependent increase in intracellular calcium in L. *minor* from 14 mGy/h, and the increased Ca^{2+} was positively correlated to the induction of ROS formation, inhibition of MMP and photosynthesis process (F_v/F_m and CO_2 uptake). This coheres well with findings that cytosolic free Ca^{2+} increased in fruits and vegetables exposed to gamma radiation (Shah, 1966). Previous studies have suggested that ROS is an important trigger for the change in intercellular Ca^{2+} level by affecting the permeable cation channels, calcium-binding domains in NADPH oxidase or endoplasmic reticulum (Schäfer and Nagy, 2006; Chaurasia et al., 2016). Increased Ca^{2+} level in chloroplasts has been suggested linked to a reduction on NAD kinase NADK2 that is involved in the synthesis of chlorophylls, $NADP^+$, and thus lead decrease in photophosphorylation (Hochmal et al., 2015). In addition, increase in intracellular Ca^{2+} may induce K^+ release in guard cells that induce stomata closure and reduction of CO_2 uptake (Allen et al., 2001). Interestingly, Ca^{2+} has been implicated in radiation-induced bystander effects where increased intracellular calcium is suggested to induce mitochondrial Ca^{2+} enrichment, reduction of the mitochondrial membrane potential, induction of ROS formation and activation of MAPK pathways involved in cell apoptosis (Lyng et al., 2006; Najafi et al., 2014). Although causal relationships between increased intracellular Ca^{2+} levels and other MoAs leading to adverse effects in *L. minor* was not clearly demonstrated herein, the potential roles in ROS formation, uncoupling of OXPHOS, regulation of stomatal closure and programmed cell death clearly warrant further studies.

4.5. Chlorophylls and total carotenoids

As the main light-harvesting pigments, chlorophyll *a* and *b* are very sensitive to environmental changes and thus reliable indicators of stress (Havaux, 2014; Hu et al., 2013). In the present study, the chlorophyll content decreased significantly at low dose rates (LOEDR = 14 mGy/h) and were associated with the inhibition of PSII performance. In chloroplast, degradation of chlorophyll in light harvesting complex II (LHC II) can directly reduce PSII efficiency, since chlorophylls are the main pigments of LHC II (Lawlor and Tezara, 2009). Moreover, loss of chlorophyll can also cause destruction of thylakoid membranes, resulting in discoloration and necrosis in plant cells (Agostinetto et al., 2016). The reduction of chlorophylls content can be potentially related to the inhibition of chlorophyll synthesis due to the gamma radiation-induced dephytolization and pheophytinization (Saha et al., 2010). Additionally, increase in chlorophyllase-mediated degradation can also reduce the chlorophyll content (Santos, 2004). The observed differences in sensitivity of chl *a* and chl *b* after exposure to gamma radiation

might thus be due to selective biosynthesis reduction or precursors degradation (Ling et al., 2008).

Total carotenoids are normally considered to be the first line of plant defence against the formation of ROS in the chloroplast which can quench $^1O2$ as well as excited chlorophyll (3Chl) through either thermal deactivation or oxidation (Ramel et al., 2012). Thus, the increase in carotenoids observed at 24 mGy/h can potentially be caused by antioxidative reactions in chloroplast, while the reduction at high dose rates might be related to gamma radiation-induced damages. In higher plants, carotenoids not only act as antioxidants, but also play as accessory pigments in light harvesting process (Hashimoto et al., 2016). The observed reduction of carotenoids can thus be causing inhibition of the light-harvesting capacity and explain some of the decrease in total photosynthesis.

4.6. Photosynthesis

4.6.1. Photosystem II (PSII) performance

Significantly decrease in PSII efficiency parameters (F_v/F_m and Φ_{PSII}) in *L. minor* were observed from 24 mGy/h after exposed to gamma radiation, whereas the EDR_{50} of Φ_{PSII} (67 mGy/h) was much lower than F_v/F_m. The decreased PSII efficiency after exposure in *L. minor* indicated PSII functioning was affected by gamma radiation. In the study by Cha-um et al. (2009), PSII efficiency was positively related chl *a* content in rice. In the present study, decreased Chl *a* observed from 14 mGy/h might be one factor triggered the PSII inhibition. Additionally, negative correlation between PSII efficiency and ROS formation was also observed and indicated the PSII inhibition in *L. minor* can be potentially due to the induction of oxidative stress in thylakoids. Previously studies have proved that decrease of PSII efficiency can be caused by the ROS-induced damage on thylakoids membranes which block electrons transport out of the receptors (D1 and D2 proteins) in PSII reaction centers (Nishiyama et al., 2011).

Photochemical quenching parameter (qP) decrease from 24 mGy/h suggested that high dose rates of gamma ration can induce a down-regulation of the open reaction centers in PSII, which directly reduce of light energy capture and electron transport to inhibit photosynthesis (Adams et al., 2013). Otherwise, decreased qP at high dose rates also verified that mechanism NPQ was not sufficient to protect the PSII from damage. Normally, NPQ protect plants from excessive light energy by dissipating it into heat (Lambrev et al., 2012). After exposure to gamma radiation, the observed decrease in NPQ at 24 mGy/h might be caused by either direct damage to the PSII reaction centres or loss of carotenoids (Frank et al., 2006; Lawlor and Tezara, 2009).

4.6.2. CO_2 uptake

In the present study, CO_2 uptake in *L. minor* significantly decreased from 14 mGy//h after 7 days of exposure. In Calvin cycle, decrease CO_2 uptake can inhibit the formation of glucose by reduce the generation of 3-phosphoglyceric acid (3-PGA) from ribulose-1,5-bisphosphate (RuBP) (Coronado-Posada et al., 2013). Positive correlation between inhibition of PSII efficiency and reduction of CO_2 uptake indicated PSII performance might partly explain the reduction of net photosynthesis as PSII performance regulated the energy generation (ATP and NADPH) for the Calvin cycle. Otherwise, reduction of CO_2 uptake positively correlated to the ROS formation as well, which suggested the oxidative stress might be also relevant for net photosynthesis. The study by Sedigheh et al. (2011) has presented that ROS increased in chloroplast can inhibit carbon fixation by induce the deactivation of Ribulose-1,5-bisphosphate carboxylase/oxygenase (Rubisco) though affect the catalytic site. Another point that deserves consideration is the stomata performance science increased Ca^{2+} can induce the stomatal closure which limit CO_2 uptake from the atmosphere (Ward and Schroeder, 1994). In the review by Gudkov et al. (2019), gamma radiation can trigger photosynthesis inhibition in terrestrial plants by influence gene expression, lipid composition of membrane, and enzymes activity in Calvin cycle. Our current results confirmed that aquatic plant *L. minor* had similar responses as terrestrial plants. In addition, the responses data from *L. minor* provided more evidence on energy supplement and cellular signaling to clarify how gamma radiation interacted photosynthesis in aquatic plant.

5. Conclusion

The presented study demonstrated that ionizing radiation displays both dose rate-dependent and target-specific responses that seems to be causally related. DNA damage and ROS production were considered the main (initiating) cellular event in *L. minor* exposed to gamma radiation, which subsequently caused a number of physiological changes leading to growth inhibition. At low dose rates, gamma radiation can induce DNA damage which reduces the frond development. At high dose rates, gamma radiation-induces ROS enhanced oxidative damage in both mitochondria and chloroplasts which may inhibit energy generation in cells and lead to growth reduction finally. For the first time, our data demonstrate that gamma radiation inhibit photosynthesis and increase Ca^{2+} level in *L. minor*. The current study proposes causal relationships between the stressor, the cellular changes occurring, and adverse effects observed and form a basis for developing a number of AOPs (AOPWiki, www.aopwiki.org) to characterize the individual steps on an AOP relevant for ionizing radiation effects in primary producers. However, there are still some gaps in knowledge such as the quantification of enzyme activity, proteins damage, energy generation in chloroplast and mitochondria together with the cell apoptosis that still require additional analysis.

Acknowledgements

Funding from the Research Council of Norway through its Centres of Excellence funding scheme, project number 223268, is gratefully acknowledged. The authors acknowledge the assistance from Dag Wenner (Norwegian University of Life Sciences) for designing the plant exposure chamber, YeonKyeong Lee (Norwegian University of Life Sciences) for the assistance of Comet assay.

Appendix A. Supplementary data

Supplementary data to this article can be found online at https://doi.org/10.1016/j.scitotenv.2019.05.016.

References

Adams, W.W., Muller, O., Cohu, C.M., Demmig-Adams, B., 2013. May photoinhibition be a consequence, rather than a cause, of limited plant productivity? Photosynth. Res. 117 (1–3), 31–44.
Ademowo, O.S., Dias, H.K.I., Burton, D.G.A., Griffiths, H.R., 2017. Lipid (per) oxidation in mitochondria: an emerging target in the ageing process? Biogerontology 18 (6), 859–879.
Agostinetto, D., Perboni, L.T., Langaro, A.C., Gomes, J., Fraga, D.S., Franco, J.J., 2016. Changes in photosynthesis and oxidative stress in wheat plants submmited to herbicides application. Planta Daninha 34 (1), 1–9.
Aldon, D., Mbengue, M., Mazars, C., Galaud, J.-P., 2018. Calcium signaling in plant biotic interactions. Int. J. Mol. Sci. 19 (3), 665.
Allen, G.J., Chu, S.P., Harrington, C.L., Schumacher, K., Hoffmann, T., Tang, Y.Y., Grill, E., Schroeder, J.I., 2001. A defined range of guard cell calcium oscillation parameters encodes stomatal movements. Nature 411 (6841), 1053.
Almeida, A.C., Gomes, T., Langford, K., Thomas, K.V., Tollefsen, K.E., 2017. Oxidative stress in the algae *Chlamydomonas reinhardtii* exposed to biocides. Aquat. Toxicol. 189, 50–59.
Asada, K., 2006. Production and scavenging of reactive oxygen species in chloroplasts and their functions. Plant Physiol. 141 (2), 391–396.
Baker, N.R., 2008. Chlorophyll fluorescence: a probe of photosynthesis in vivo. Annu. Rev. Plant Biol. 59, 89–113.
Bjerke, H., Hetland, P.O., 2014. Dosimetri ved FIGARO gammaanlegget ved NMBU, Ås: Målerapport fra oppmåling av doseraten i strålefeltet fra kobolt-60.
Bowen, H., Cawse, P., Smith, S., 1962. The effects of low doses of gamma radiation on plant yields. The International Journal of Applied Radiation and Isotopes 13 (9), 487–492.
Cha-Um, S., et al., 2009. Sugar accumulation, photosynthesis and growth of two indica rice varieties in response to salt stress. Acta Physiol. Plant. 31 (3), 477–486.
Chaurasia, M., Bhatt, A.N., Das, A., Dwarakanath, B.S., Sharma, K., 2016. Radiation-induced autophagy: mechanisms and consequences. Free Radic. Res. 50 (3), 273–290.

Cheloni, G., Slaveykova, V.I., 2013. Optimization of the C11-BODIPY581/591 dye for the determination of lipid oxidation in *Chlamydomonas reinhardtii* by flow cytometry. Cytometry Part A 83 (10), 952–961.
Choudhury, S., Panda, P., Sahoo, L., Panda, S.K., 2013. Reactive oxygen species signaling in plants under abiotic stress. Plant Signal. Behav. 8 (4), e23681.
Coronado-Posada, N., Cabarcas-Montalvo, M., Olivero-Verbel, J., 2013. Phytotoxicity assessment of a methanolic coal dust extract in *Lemna minor*. Ecotoxicol. Environ. Saf. 95, 27–32.
Ehrenberg, B., Montana, V., Wei, M., Wuskell, J., Loew, L., 1988. Membrane potential can be determined in individual cells from the nernstian distribution of cationic dyes. Biophys. J. 53 (5), 785–794.
Frank, H.A., Young, A., Britton, G., Cogdell, R.J., 2006. The Photochemistry of Carotenoids. Springer Netherlands.
Garnier-Laplace, J., Geras'kin, S., Della-Vedova, C., Beaugelin-Seiller, K., Hinton, T.G., Real, A., Oudalova, A., 2013. Are radiosensitivity data derived from natural field conditions consistent with data from controlled exposures? A case study of Chernobyl wildlife chronically exposed to low dose rates. J. Environ. Radioact. 121, 12–21.
Geras'kin, S.A., 2016. Ecological effects of exposure to enhanced levels of ionizing radiation. J. Environ. Radioact. 162, 347–357.
Geras'kin, S.A., Fesenko, S.V., Alexakhin, R.M., 2008. Effects of non-human species irradiation after the Chernobyl NPP accident. Environ. Int. 34 (6), 880–897.
Gichner, T., Patková, Z., Száková, J., Demnerová, K., 2004. Cadmium induces DNA damage in tobacco roots, but no DNA damage, somatic mutations or homologous recombination in tobacco leaves. Mutation Research/Genetic Toxicology and Environmental Mutagenesis 559 (1), 49–57.
Gilbin, R., Alonzo, F., Garnier-Laplace, J., 2008. Effects of chronic external gamma irradiation on growth and reproductive success of Daphnia magna. J. Environ. Radioact. 99 (1), 134–145.
Gomes, T., Xie, L., Brede, D., Lind, O.-C., Solhaug, K.A., Salbu, B., Tollefsen, K.E., 2017. Sensitivity of the green algae *Chlamydomonas reinhardtii* to gamma radiation: photosynthetic performance and ROS formation. Aquat. Toxicol. 183, 1–10.
González, L.N., Arruda-Neto, J.D.T., Cotta, M.A., Carrer, H., Garcia, F., Silva, R.A.S., Moreau, A.L.D., Righi, H., Genofre, G.C., 2012. DNA fragmentation by gamma radiation and electron beams using atomic force microscopy. J. Biol. Phys. 38 (3), 531–542.
Greenberg, J.T., Demple, B., 1986. Glutathione in Escherichia coli is dispensable for resistance to H2O2 and gamma radiation. J. Bacteriol. 168 (2), 1026–1029.
Gudkov, S.V., Grinberg, M.A., Sukhov, V., Vodeneev, V., 2019. Effect of ionizing radiation on physiological and molecular processes in plants. J. Environ. Radioact. 202, 8–24.
Gyori, B.M., Venkatachalam, G., Thiagarajan, P., Hsu, D., Clement, M.-V., 2014. OpenComet: an automated tool for comet assay image analysis. Redox Biol. 2, 457–465.
Halliwell, B., 1987. Oxidative damage, lipid peroxidation and antioxidant protection in chloroplasts. Chem. Phys. Lipids 44 (2–4), 327–340.
Hameed, A., Shah, T.M., Atta, B.M., Haq, M.A., Sayed, H., 2008. Gamma irradiation effects on seed germination and growth, protein content, peroxidase and protease activity, lipid peroxidation in desi and kabuli chickpea. Pak. J. Bot. 40 (3), 1033–1041.
Harrison, F.L., Anderson, S.L., 1996. Taxonomic and Developmental Aspects of Radiosensitivity (No. UCRL-JC-125920; CONF-960529-1). Lawrence Livermore National Lab, CA (United States).
Hashimoto, H., Uragami, C., Cogdell, R.J., 2016. In: Stange, C. (Ed.), Carotenoids in Nature: Biosynthesis, Regulation and Function. Springer International Publishing, Cham, pp. 111–139.
Haugland, R.P., 2005. The Handbook: A Guide to Fluorescent Probes and Labeling Technologies.
Havaux, M., 2014. Carotenoid oxidation products as stress signals in plants. Plant J. 79 (4), 597–606.
Hevrøy, T.H., Golz, A.L., Xie, L., Hansen, E.L., Bradshaw, C., 2019. Radiation effects and ecological processes in a freshwater microcosm. J. Environ. Radioact. 203, 71–83.
Hiyama, A., Nohara, C., Kinjo, S., Taira, W., Gima, S., Tanahara, A., Otaki, J.M., 2012. The biological impacts of the Fukushima nuclear accident on the pale grass blue butterfly. Sci. Rep. 2, 570.
Hochmal, A.K., Schulze, S., Trompelt, K., Hippler, M., 2015. Calcium-dependent regulation of photosynthesis. Biochimica et Biophysica Acta (BBA) - Bioenergetics 1847 (9), 993–1003.
Hodgson, G.L., 1970. Effects of temperature on the growth and development of *Lemna minor*, under conditions of natural daylight. Ann. Bot. 34 (2), 365–381.
Hu, Z., Li, H., Chen, S., Yang, Y., 2013. Chlorophyll content and photosystem II efficiency in soybean exposed to supplemental ultraviolet-B radiation. Photosynthetica 51 (1), 151–157.
Hulsen, K., Minne, V., Lootens, P., Vandecasteele, P., Höfte, M., 2002. A chlorophyll a fluorescence-based *Lemna minor* bioassay to monitor microbial degradation of nanomolar to micromolar concentrations of linuron. Environ. Microbiol. 4 (6), 327–337.
Imlay, J.A., Linn, S., 1988. DNA damage and oxygen radical toxicity. Science 240 (4857), 1302–1309.
Jamers, A.N., Lenjou, M., Deraedt, P., Bockstaele, D.V., Blust, R., Coen, W.d., 2009. Flow cytometric analysis of the cadmium-exposed green alga *Chlamydomonas reinhardtii* (Chlorophyceae). Eur. J. Phycol. 44 (4), 541–550.
Kovacs, E., Keresztes, A., 2002. Effect of gamma and UV-B/C radiation on plant cells. Micron 33 (2), 199–210.
Kozuleva, M.A., Ivanov, B.N., 2016. The mechanisms of oxygen reduction in the terminal reducing segment of the chloroplast photosynthetic electron transport chain. Plant Cell Physiol. 57 (7), 1397–1404.
Kryshev, I., Sazykina, T., 1998. Radioecological effects on aquatic organisms in the areas with high levels of radioactive contamination: environmental protection criteria. Radiat. Prot. Dosim. 75 (1–4), 187–191.
Lambrev, P.H., Miloslavina, Y., Jahns, P., Holzwarth, A.R., 2012. On the relationship between non-photochemical quenching and photoprotection of photosystem II. Biochimica et Biophysica Acta (BBA)-Bioenergetics 1817 (5), 760–769.
Landolt, E., Kandeler, R., 1987. Biosystematic Investigations in the Family of Duckweeds (Lemnaceae), Vol. 4: The Family of Lemnaceae-a Monographic Study, Vol. 2 (Phytochemistry, Physiology, Application, Bibliography). Veroeffentlichungen des Geobotanischen Instituts der ETH, Stiftung Ruebel, Switzerland.
LaVerne, J.A., 2000. OH radicals and oxidizing products in the gamma radiolysis of water. Radiat. Res. 153 (2), 196–200.
Lawlor, D.W., Tezara, W., 2009. Causes of decreased photosynthetic rate and metabolic capacity in water-deficient leaf cells: a critical evaluation of mechanisms and integration of processes. Ann. Bot. 103 (4), 561–579.
Li, W., Xu, F., Chen, S., Zhang, Z., Zhao, Y., Jin, Y., Li, M., Zhu, Y., Liu, Y., Yang, Y., 2014. A comparative study on Ca content and distribution in two Gesneriaceae species reveals distinctive mechanisms to cope with high rhizospheric soluble calcium. Front. Plant Sci. 5, 647.
Lichtenthaler, H.K., 1987. Chlorophylls and carotenoids: pigments of photosynthetic biomembranes. Methods in Enzymology. Elsevier, pp. 350–382.
Lichtenthaler, H.K., Buschmann, C., 2001. Chlorophylls and carotenoids: measurement and characterization by UV-VIS spectroscopy. Current protocols in food analytical chemistry 1 (1) (F4-3).
Liemburg-Apers, D.C., Willems, P.H.G.M., Koopman, W.J.H., Grefte, S., 2015. Interactions between mitochondrial reactive oxygen species and cellular glucose metabolism. Arch. Toxicol. 89 (8), 1209–1226.
Lind, O.C., Helen Oughton, D., Salbu, B., 2019. The NMBU FIGARO low dose irradiation facility. Int. J. Radiat. Biol. 95 (1), 76–81.
Ling, A., Kiong, P., Grace Lai, A., Hussein, S., Harun, A.R., 2008. Physiological responses of Orthosiphon stamineus plantles to gamma irradiation. American-Eurasian journal of sustainable agriculture 2 (2), 135–149.
Liochev, S.I., Fridovich, I., 1994. The role of O_2^- in the production of HO.: in vitro and in vivo. Free Radic. Biol. Med. 16 (1), 29–33.
Lyng, F.M., Maguire, P., McClean, B., Seymour, C., Mothersill, C., 2006. The involvement of calcium and MAP kinase signaling pathways in the production of radiation-induced bystander effects. Radiat. Res. 165 (4), 400–409.
Machado, M.D., Soares, E.V., 2012. Assessment of cellular reduced glutathione content in *Pseudokirchneriella subcapitata* using monochlorobimane. J. Appl. Phycol. 24 (6), 1509–1516.
Manova, V., Gruszka, D., 2015. DNA damage and repair in plants – from models to crops. Front. Plant Sci. 6, 885.
Martínez-Reyes, I., Cuezva, J.M., 2014. The H^+-ATP synthase: a gate to ROS-mediated cell death or cell survival. Biochimica et Biophysica Acta (BBA)-Bioenergetics 1837 (7), 1099–1112.
Mazars, C., Thuleau, P., Lamotte, O., Bourque, S., 2010. Cross-talk between ROS and calcium in regulation of nuclear activities. Mol. Plant 3 (4), 706–718.
McCabe, J., Shelp, B., Ursino, D.J., 1979. Photosynthesis and photophosphorylation in radiation-stressed soybean plants and the relation of these processes to photoassimilate export. Environ. Exp. Bot. 19 (4), 253–261.
McLay, C.L., 1976. The effect of pH on the population growth of three species of duckweed: Spirodela oligorrhiza, *Lemna minor* and Wolffia arrhiza. Freshw. Biol. 6 (2), 125–136.
Mehler, H.A., 1951. Studies on reactions of illuminated chloroplasts. I. Mechanism of the reduction of oxygen and other Hill reagents. Arch. Biochem. Biophys. 33, 65–77.
Miller, M.O., Miller, D.A., 2016. The technological enhancement of normally occurring radioactive materials in red mud due to the production of alumina. International Journal of Spectroscopy 2016.
Møller, A.P., Nishiumi, I., Suzuki, H., Ueda, K., Mousseau, T.A., 2013. Differences in effects of radiation on abundance of animals in Fukushima and Chernobyl. Ecol. Indic. 24, 75–81.
Nair, R., Sunny, F., Chopra, M., Sharma, L., Puranik, V., Ghosh, A., 2014. Estimation of radioactive leakages into the Pacific Ocean due to Fukushima nuclear accident. Environ. Earth Sci. 71 (3), 1007–1019.
Najafi, M., Fardid, R., Hadadi, G., Fardid, M., 2014. The mechanisms of radiation-induced bystander effect. Journal of Biomedical Physics & Engineering 4 (4), 163–172.
Nishiyama, Y., Allakhverdiev, S.I., Murata, N., 2011. Protein synthesis is the primary target of reactive oxygen species in the photoinhibition of photosystem II. Physiol. Plant. 142 (1), 35–46.
Noctor, G., Mhamdi, A., Chaouch, S., Han, Y.I., Neukermans, J., Marquez-Garcia, B., Queval, G., Foyer, C.H., 2012. Glutathione in plants: an integrated overview. Plant Cell Environ. 35 (2), 454–484.
OECD, 2006. Test No. 221: Lemna Sp. Growth Inhibition Test. OECD Publishing.
Panda, S.K., Yamamoto, Y., Kondo, H., Matsumoto, H., 2008. Mitochondrial alterations related to programmed cell death in tobacco cells under aluminium stress. C R Biol 331 (8), 597–610.
Ramachandran, T.V., 2011. Background radiation, people and the environment. International Journal of Radiation Research 9 (2), 63.
Ramel, F., Birtic, S., Cuiné, S., Triantaphylidès, C., Ravanat, J.-L., Havaux, M., 2012. Chemical quenching of singlet oxygen by carotenoids in plants. Plant Physiol. 158 (3), 1267–1278.
Razinger, J., Drinovec, L., Zrimec, A., 2010. Real-time visualization of oxidative stress in a floating macrophyte *Lemna minor* L. exposed to cadmium, copper, menadione, and AAPH. Environ. Toxicol. 25 (6), 573–580.
Real, A., Sundell-Bergman, S., Knowles, J., Woodhead, D., Zinger, I., 2004. Effects of ionising radiation exposure on plants, fish and mammals: relevant data for environmental radiation protection. J. Radiol. Prot. 24 (4A), A123.
Reisz, J.A., Bansal, N., Qian, J., Zhao, W., Furdui, C.M., 2014. Effects of ionizing radiation on biological molecules—mechanisms of damage and emerging methods of detection. Antioxid. Redox Signal. 21 (2), 260–292.

Saha, P., Raychaudhuri, S.S., Chakraborty, A., Sudarshan, M., 2010. PIXE analysis of trace elements in relation to chlorophyll concentration in Plantago ovata Forsk. Appl. Radiat. Isot. 68 (3), 444–449.
Santos, C.V., 2004. Regulation of chlorophyll biosynthesis and degradation by salt stress in sunflower leaves. Sci. Hortic. 103 (1), 93–99.
Scaduto, R.C., Grotyohann, L.W., 1999. Measurement of mitochondrial membrane potential using fluorescent rhodamine derivatives. Biophys. J. 76 (1), 469–477.
Schäfer, E., Nagy, F., 2006. Photomorphogenesis in Plants and Bacteria: Function and Signal Transduction Mechanisms. Springer, Netherlands.
Sedigheh, H.G., Mortazavian, M., Norouzian, D., Atyabi, M., Akbarzadeh, A., Hasanpoor, K., Ghorbani, M., 2011. Oxidative stress and leaf senescence. BMC research notes 4 (1), 477.
Severi, A., Fornasiero, R.B., 1983. Morphological variations in *Lemna minor* L. and possible relationships with abscisic acid. Caryologia 36 (1), 57–64.
Shadyro, O.I., Yurkova, I.L., Kisel, M.A., 2002. Radiation-induced peroxidation and fragmentation of lipids in a model membrane. Int. J. Radiat. Biol. 78 (3), 211–217.
Shah, J., 1966. Radiation-induced calcium release and its relation to post-irradiation textural changes in fruits and vegetables. Nature 211 (5050), 776.
Teoule, R., 1987. Radiation-induced DNA damage and its repair. International Journal of Radiation Biology and Related Studies in Physics, Chemistry and Medicine 51 (4), 573–589.
Thormar, J., Hasler-Sheetal, H., Baden, S., Boström, C., Clausen, K.K., Krause-Jensen, D., Olesen, B., Rasmussen, J.R., Svensson, C.J., Holmer, M., 2016. Eelgrass (Zostera marina) food web structure in different environmental settings. PLoS One 11 (1), e0146479.
Tripathy, B.C., Oelmüller, R., 2012. Reactive oxygen species generation and signaling in plants. Plant Signal. Behav. 7 (12), 1621–1633.
Tuteja, N., Mahajan, S., 2007. Calcium signaling network in plants: an overview. Plant Signal. Behav. 2 (2), 79–85.
Van Hoeck, A., Horemans, N., Van Hees, M., Nauts, R., Knapen, D., Vandenhove, H., Blust, R., 2015. Characterizing dose response relationships: chronic gamma radiation in *Lemna minor* induces oxidative stress and altered polyploidy level. J. Environ. Radioact. 150, 195–202.
Vanhoudt, N., Vandenhove, H., Horemans, N., Wannijn, J., Van Hees, M., Vangronsveld, J., Cuypers, A., 2010. The combined effect of uranium and gamma radiation on biological responses and oxidative stress induced in Arabidopsis thaliana. J. Environ. Radioact. 101 (11), 923–930.
Vidaković Cifrek, Ž., Sorić, S., Babić, M., 2013. Growth and photosynthesis of *Lemna minor* L. exposed to different light conditions and sucrose supplies. Acta Botanica Croatica 72 (2), 211–219.
Wada, T., Fujita, T., Nemoto, Y., Shimamura, S., Mizuno, T., Sohtome, T., Kamiyama, K., Narita, K., Watanabe, M., Hatta, N., 2016. Effects of the nuclear disaster on marine products in Fukushima: an update after five years. J. Environ. Radioact. 164, 312–324.
Ward, J.M., Schroeder, J.I., 1994. Calcium-activated K^+ channels and calcium-induced calcium release by slow vacuolar ion channels in guard cell vacuoles implicated in the control of stomatal closure. Plant Cell 6 (5), 669–683.
Wi, S.G., Chung, B.Y., Kim, J.-S., Kim, J.-H., Baek, M.-H., Lee, J.-W., Kim, Y.S., 2007. Effects of gamma irradiation on morphological changes and biological responses in plants. Micron 38 (6), 553–564.
Xie, L., Gomes, T., Solhaug, K.A., Song, Y., Tollefsen, K.E., 2018. Linking mode of action of the model respiratory and photosynthesis uncoupler 3, 5-dichlorophenol to adverse outcomes in *Lemna minor*. Aquat. Toxicol. 197, 98–108.
Zorov, D.B., Juhaszova, M., Sollott, S.J., 2014. Mitochondrial reactive oxygen species (ROS) and ROS-induced ROS release. Physiol. Rev. 94 (3), 909–950.
Zorova, L.D., Popkov, V.A., Plotnikov, E.Y., Silachev, D.N., Pevzner, I.B., Jankauskas, S.S., Babenko, V.A., Zorov, S.D., Balakireva, A.V., Juhaszova, M., Sollott, S.J., Zorov, D.B., 2018. Mitochondrial membrane potential. Anal. Biochem. 552, 50–59.